AUPET Press
Technical Journal of Daukeyev University
Volume 1, Issue 1, 2021, pp. 57-68
ISSN 2788-5488

Three-Dimensional Motion of Tennis Ball

Anastas Ivanov Ivanov
Todor Kableshkov University of Transport, Sofia 1574, Bulgaria
Corresponding author: Anastas Ivanov Ivanov; aii2010@abv.bg
Received: 23 May 2021; Accepted: 29 May 2021; Published: 31 May 2021
DOI: https://doi.org/10.52542/tjdu.1.1.57-68

Abstract. Modern tennis players use a variety of strokes. From the physical point of view, these shots can be classified into eight main groups depending on the way the racket interacts with the tennis ball. These are strokes with top, bottom, side, top-side, and bottom-side rotation, as well as strokes without rotation. These eight interactions lead to eight main types of trajectories at the same initial position and the same initial linear velocity. The main purpose of the study is to determine these trajectories and to describe their advantages and disadvantages in modern competitive tennis. The calculations and graphical images are performed with the MatLab mathematical package.

Keywords: tennis balls, 3D motion, magnus effect, numerical solution, MatLab.

1. Introduction

The origin of tennis was born in France around the 12th century. The origin of modern tennis was invented by Major Walter Wingfield, an army officer of Wales in 1873. In 1853, the German physicist Gustav Magnus published two articles explaining the deflection of the projectile and rotating bodies [1-2]. However, in 1672, Isaac Newton had described this phenomenon and correctly inferred the cause after observing tennis players in the Cambridge College [3]. In 1742, Benjamin Robins, a British mathematician, ballistics researcher, and military engineer, explained deviations in the trajectories of musket balls in terms of the Magnus effect [4]. In recent years, there has been a significant increase in researches related to the motion and flight of a variety of sports balls in a real fluid environment, including tennis balls. For example, such studies could be seen in the works [5-11]. The effect of spin using experimental and computational methods is studied in the work [12]. The simulation results are compared with experimental findings. The measurements of drag and lift on new tennis balls in flight are presented in the study [13]. Two video cameras are used to measure the velocity and flight height of the balls. They are fired from a ball launcher at a velocity between 15 and 30 m/s and with topspin or backspin at rates up to 2000 rpm. The studies of spinning and non-spinning tennis ball aerodynamics, and the determining of the drag and lift coefficients, are made in the publications [14-17]. A three-dimensional study of tennis ball flight is done in the study [18], where a classical analytical formula is used for the lift coefficient. All tennis strokes can be classified into eight main groups depending on how the racket interacts with the tennis ball. These are strokes with top, bottom, side, top-side, and bottom-side rotation, as well as strokes without rotation. These eight interactions lead to eight characteristic types of trajectories at the same initial position and the same initial velocities. The main purpose of the study is to study these trajectories and to describe their parameters with a view to their use in modern competitive tennis.

2. Dynamical model

The tennis ball is a round, hollow, several-layered sphere with a certain average thickness. The ball is an elastic body with strong damping characteristics. The air inside the competition balls is under pressure higher than atmospheric. A fluffy woolen knit is glued on the rubber surface of the ball (Figure 1 and Figure 2).

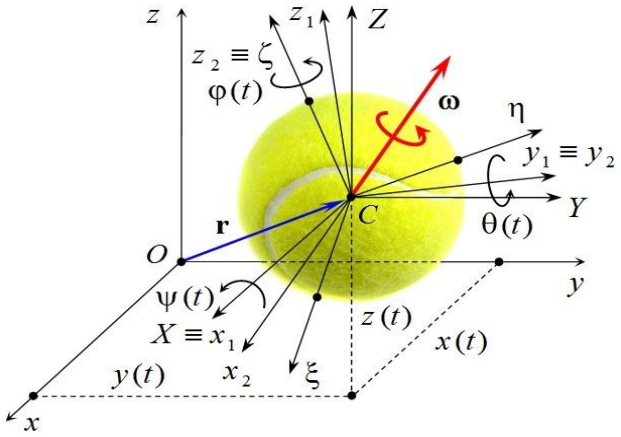

Figure 1. Generalized coordinates.

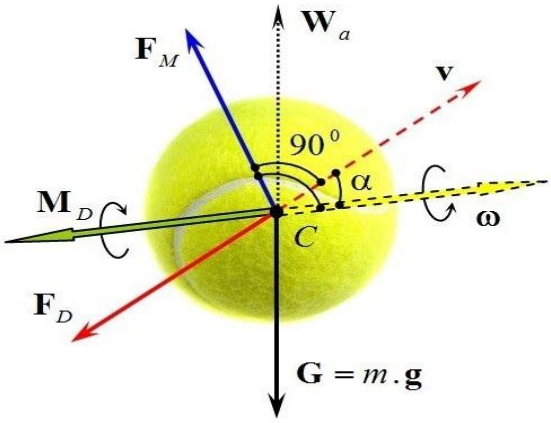

Figure 2. Aerodynamic forces.

The ball is assumed to be a perfectly rigid hollow closed two-layer spherical shell. The rubber wall is defined by an inner radius $r = 0.026\ m$ and an outer radius $R_1 = 0.030\ m$. Wool knit gives the total size of the ball with a radius $R = 0.0325\ m$. The main physical characteristics of the tennis ball are: the mass of the tire $m_1 = 0.045\ kg$, the mass of the knit $m_2 = 0.012\ kg$, the total mass $m = m_1 + m_2$, and the mass moment of inertia $J = 3.155 \times 10^{-5}\ kg.m^2$. The flight of a tennis ball is represented as a general motion of a hollow spherical rigid body in an air environment, the influence of which is taken into account with aerodynamic forces.

3. Differential equations

The law of motion of the tennis ball represents the six functions: $x(t)$, $y(t)$, $z(t)$, $\psi(t)$, $\theta(t)$ and $\varphi(t)$, (see Figure 1). They are included in the both vectors:

$$\mathbf{r} = \langle\, x(t) \quad y(t) \quad z(t) \,\rangle^T \tag{1}$$

$$\mathbf{p} = \langle\, \psi(t) \quad \theta(t) \quad \varphi(t) \,\rangle^T \tag{2}$$

The rotation speed of a tennis ball is described by the angular velocity vector:

$$\boldsymbol{\omega} = \langle\, \omega_X \quad \omega_Y \quad \omega_Z \,\rangle^T \tag{3}$$

The two vectors $\mathbf{p}$ and $\boldsymbol{\omega}$ are related with the following kinematical equation:

$$\boldsymbol{\omega} = \mathbf{S}.\mathbf{p} \tag{4}$$

The matrix $\mathbf{S}$, when the Cardan angles are used, has the form:

$$\mathbf{S} = \begin{bmatrix} 1 & 0 & \sin\theta \\ 0 & \cos\psi & -\cos\theta.\sin\psi \\ 0 & \sin\psi & \cos\theta.\cos\psi \end{bmatrix} \tag{5}$$

The system of differential equations, presented in vector-matrix form, which determines the law of motion of the tennis ball, has the form:

$$m.\ddot{\mathbf{r}} = \mathbf{F} \tag{6}$$

$$J.\left(\mathbf{S}.\ddot{\mathbf{p}}+\dot{\mathbf{S}}.\dot{\mathbf{p}}\right)=\mathbf{M} \tag{7}$$

where $\mathbf{F}$ and $\mathbf{M}$ are the main force and the main moment of all forces acting on the tennis ball. They are reduced to its mass center C, (Figure 2).

The main force $\mathbf{F}$ is a vector sum of three forces:

$$\mathbf{F}=\mathbf{F}_g+\mathbf{F}_D+\mathbf{F}_L \tag{8}$$

The force $\mathbf{F}_g$ is a vector sum between the weight of the tennis ball $\mathbf{G}$ and the lifting force $\mathbf{W}_a$ according to Archimedes law, (Figure 2). It is determined by the formula:

$$\mathbf{F}_g=\mathbf{G}+\mathbf{W}_a=\left(m-V.\rho\right).\mathbf{g} \tag{9}$$

where V is the volume of the tennis ball, ρ is the density of the air, and $\mathbf{g}$ is the ground acceleration.

The density of the air is strongly influenced by temperature. For this study, the air density is taken as the average value $\rho=1.205\,kg/m^3$ at $t=20^oC$. The earth acceleration vector has the form:

$$\mathbf{g}=\left\langle 0 \quad 0 \quad -g \right\rangle^T \tag{10}$$

and for average latitudes, the magnitude of earth acceleration is assumed $g=9.81\,m/s^2$.

In fact, for the tennis balls, the Archimedes lift force can be neglected.

The force $\mathbf{F}_D$ is the resistance force, (Figure 2). It is one of the main aerodynamic forces. It is determined by the formula:

$$\mathbf{F}_D=\frac{1}{2}.C_D.A.\rho.\left|\dot{\mathbf{r}}\right|.\dot{\mathbf{r}} \tag{11}$$

where A is the area of the middle section of the tennis ball.

The drag coefficient C_D is considered to be a turbulent flow regime [13-16]. When the tennis balls are flying at medium velocities, this coefficient retains a relatively constant value for a wide range of Reynolds numbers, namely $5\times10^4\le R_e\le 7.5\times10^4\ m^2/s$.

The other main aerodynamic force is the Magnus force, (see Figure 2). It is determined by the formula:

$$\mathbf{F}_L=\frac{1}{2}.C_L.A.\rho.v^2.\frac{\boldsymbol{\Omega}.\dot{\mathbf{r}}}{\left|\boldsymbol{\Omega}.\dot{\mathbf{r}}\right|} \tag{12}$$

In Eq. (12), the matrix $\boldsymbol{\Omega}$ is constructed from the components of the angular velocity vector $\boldsymbol{\omega}$ and has the form:

$$\boldsymbol{\Omega}=\begin{bmatrix} 0 & -\omega_Z & \omega_Y \\ \omega_Z & 0 & -\omega_X \\ -\omega_Y & \omega_X & 0 \end{bmatrix} \tag{13}$$

The lift coefficient C_L of Magnus, for the same turbulent flow regime, $5\times10^4 \le R_e \le 7.5\times10^4\ m^2/s$, depends not only on the Reynolds numbers, but also on the spin parameter S. When the spin parameter S is increased, the value of lift coefficient C_L is also increased. This phenomena is clearly described in the works [13-16]. For this study, the spin parameter is assumed with the value:

$$S = \frac{\omega.R}{v} = \frac{150\times0.0325}{30} = 0.1625 \tag{14}$$

The main moment coincides with the drag aerodynamic moment as follows:

$$\mathbf{M} \equiv \mathbf{M}_D = \frac{1}{2}.C_M.A.\rho.v^2.\frac{\boldsymbol{\Omega}}{|\boldsymbol{\Omega}|} \tag{15}$$

The coefficient C_M depends on the Reynolds number, the spin rate, and the condition of the uniform felt the fabric of the tennis ball, and in particular, whether the balls are new or old with a thin knit. The study, which is shown on the next pages, is performed with the following values: $C_D = 0.50$, $C_L = 0.20$, and $C_M = 0.01$.

4. Numerical solution

For the numerical solution of the system of differential Eq. (6) and Eq. (7) in the time area, the program using MatLab is prepared.

The laws of motion, velocities and accelerations for all generalized coordinates are obtained, as well as the laws of velocity and acceleration of the mass center of the ball: $x(t)$, $y(t)$, $z(t)$, $\psi(t)$, $\psi(t)$, $\theta(t)$, $\varphi(t)$, $\dot{x}(t)\equiv v_x$, $\dot{y}(t)\equiv v_y$, $\dot{z}(t)\equiv v_z$, $\dot{\psi}(t)$, $\dot{\theta}(t)$, $\dot{\varphi}(t)$, $\ddot{x}(t)\equiv a_x$, $\ddot{y}(t)\equiv a_y$, $\ddot{z}(t)\equiv a_z$, $\ddot{\psi}(t)$, $\ddot{\theta}(t)$, $\ddot{\varphi}(t)$.

The laws of angular velocity and angular acceleration of the tennis ball are obtained, namely: $\omega_x(t)$, $\omega_y(t)$, $\omega_z(t)$, $\varepsilon_x(t)\equiv\dot{\omega}_x(t)$, $\varepsilon_y(t)\equiv\dot{\omega}_y(t)$, $\varepsilon_z(t)\equiv\dot{\omega}_z(t)$.

Finally, the projections of the trajectory of the mass center of the tennis ball on the three coordinate planes, Oxz, Oyz and Oxy are obtained. The calculations were performed with the following initial conditions.

Initial position: $x_0 = y_0 = 0$, $z_0 = 1.00\ m$, $\psi_0 = \theta_0 = \varphi_0 = 0$.

The tennis ball is fired at an initial velocity $v_0 = 30\ m/s$ at an angle $\alpha = 6^0$ towards the horizon. The projections of the velocity v_0 define the initial linear velocities, namely: $\dot{x}_0 = 29.836\ m/s$, $\dot{y}_0 = 0$ and $\dot{z}_0 = 3.136\ m/s$. Eight types of strokes, depending on the initial angular velocities, are studied. These strokes and the corresponding initial angular velocities are shown in Figures 3-34. In these figures, the red elliptical areas indicate the places where the tennis racket must brush the ball to give it the angular velocity.

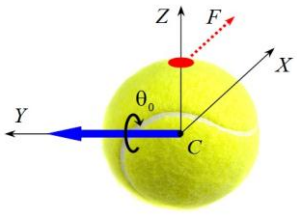

Figure 3. Topspin stroke: $\theta_0 = 150\ s^{-1} \equiv 942.5$ rpm.

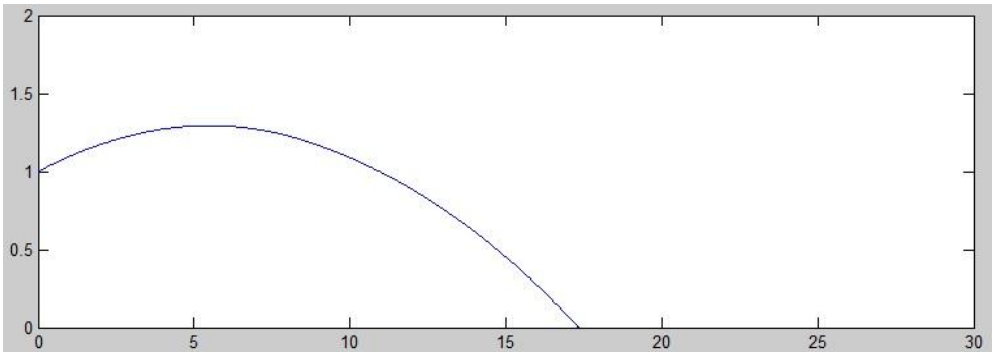

Figure 4. Projection of the trajectory in Oxz plane.

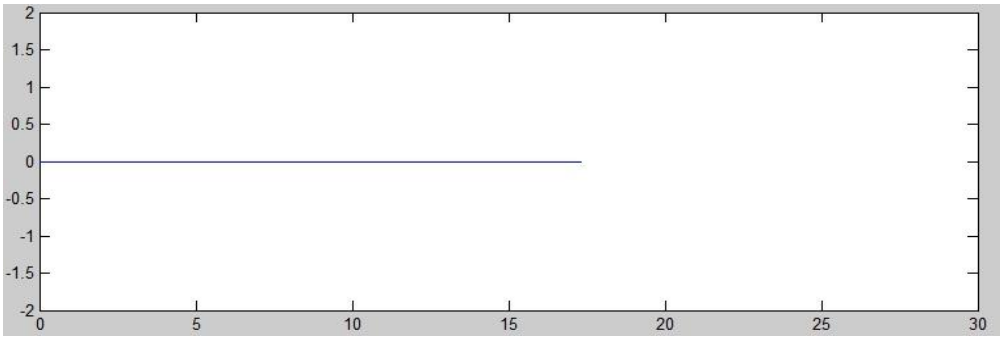

Figure 5. Projection of the trajectory in Oxy plane.

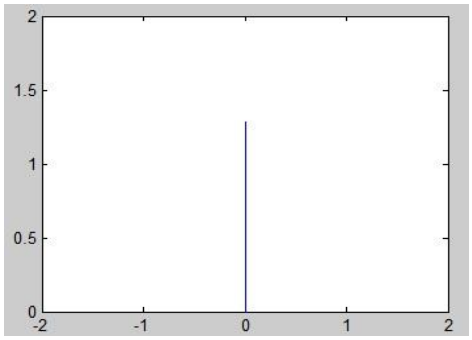

Figure 6. Projection of the trajectory in Oyz plane.

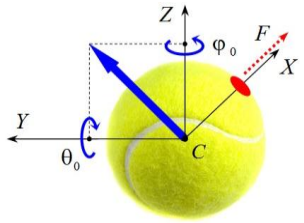

Figure 7. Right topspin stroke: $\theta_0 = 106.066\ s^{-1}$, $\varphi_0 = 106.066\ s^{-1}$.

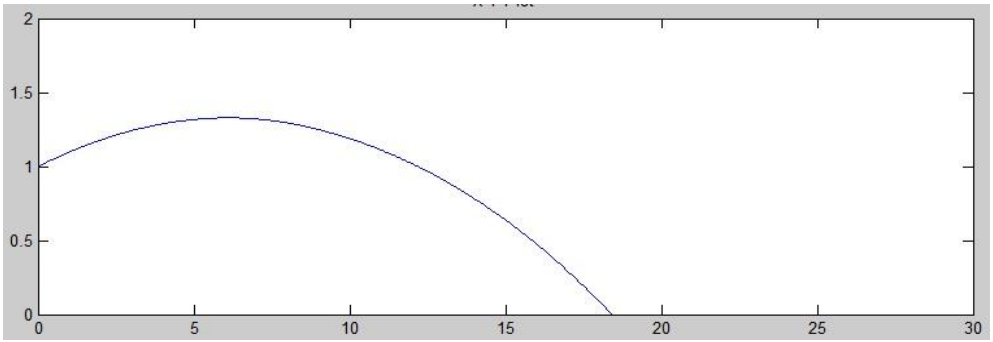

Figure 8. Trajectory in Oxz plane: $\max X = 18.420\ m$, $\max Z = 1.329\ m$.

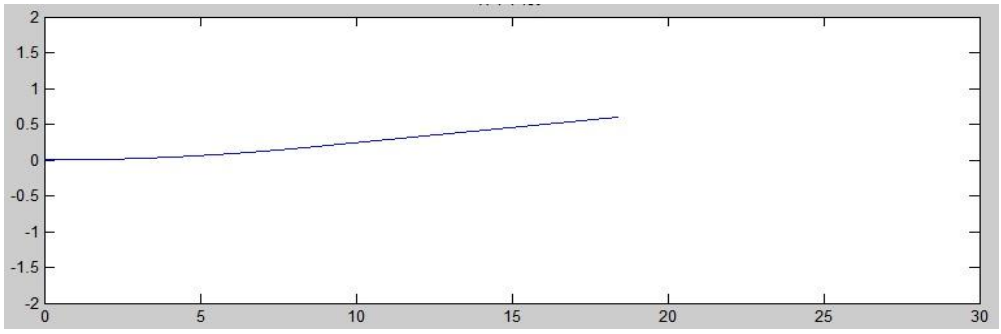

Figure 9. Trajectory in Oxy plane: $\max X = 18.420\ m$, $\max Y = 0.599\ m$.

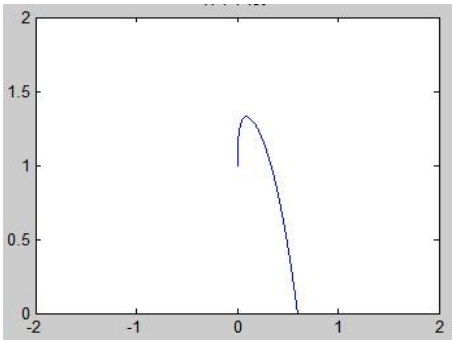

Figure 10. Trajectory in Oyz plane: $\max Y = 0.599\ m$, $\max Z = 1.329\ m$.

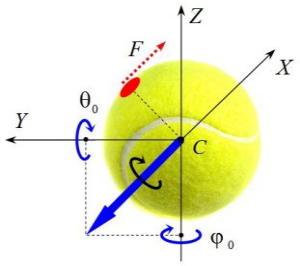

Figure 11. Left topspin stroke: $\theta_0 = 106.066\ s^{-1}$, $\varphi_0 = -106.066\ s^{-1}$.

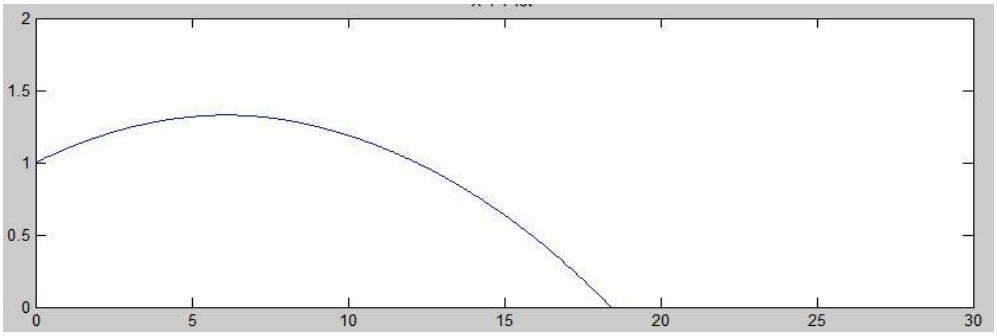

Figure 12. Trajectory in Oxz plane: $\max X = 18.420\ m$, $\max Z = 1.329\ m$.

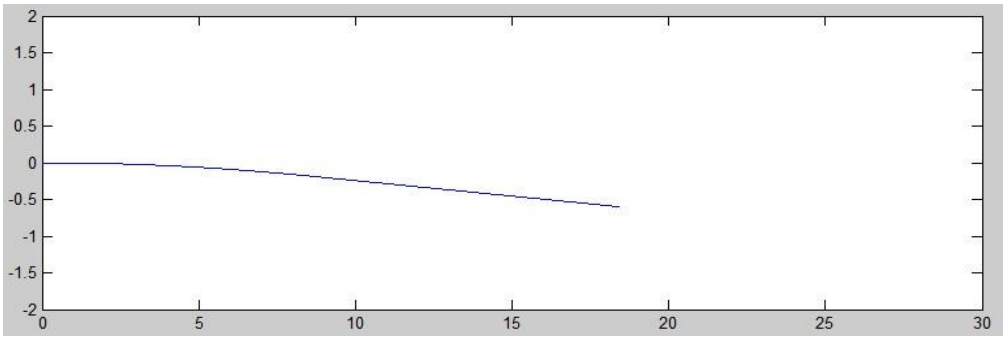

Figure 13. Trajectory in Oxy plane: $\max X = 18.420\ m$, $\min Y = -0.599\ m$.

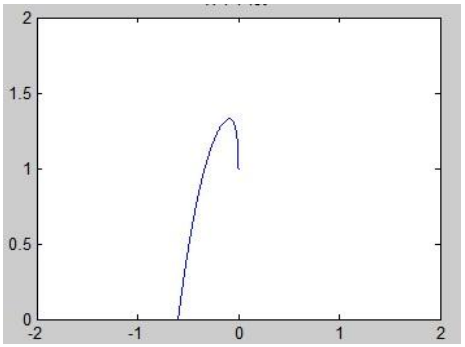

Figure 14. Trajectory in Oyz plane: $\min Y = -0.599\ m$, $\max Z = 1.329\ m$.

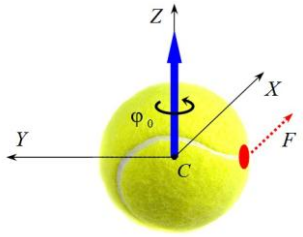

Figure 15. Side right-spin stroke: $\theta_0 = 150\ s^{-1} \equiv 942.5$ rpm.

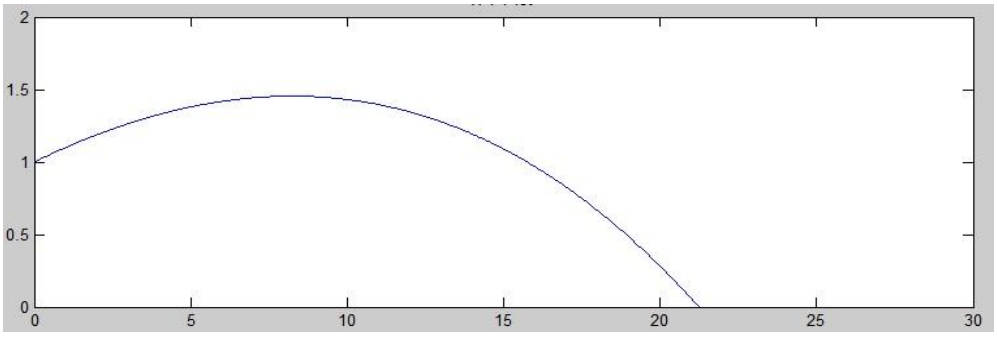

Figure 16. Trajectory in Oxz plane: $\max X = 21.237\ m$, $\max Z = 1.454\ m$.

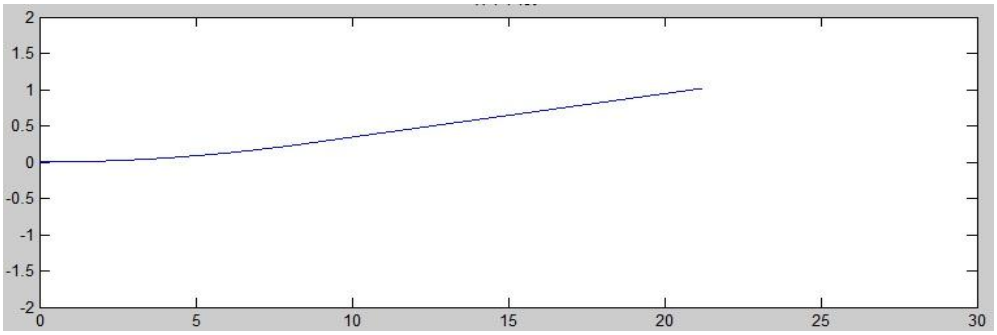

Figure 17. Trajectory in Oxy plane: $\max X = 21.237\ m$, $\max Y = 1.018\ m$.

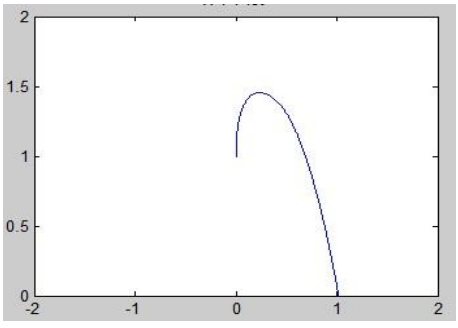

Figure 18. Trajectory in Oyz plane: $\max Y = 1.018\ m$, $\max Z = 1.454\ m$.

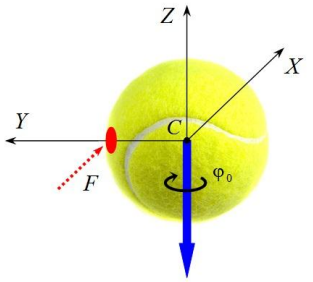

Figure 19. Side left-spin stroke: $\theta_0 = 150\ s^{-1} \equiv 942.5$ rpm.

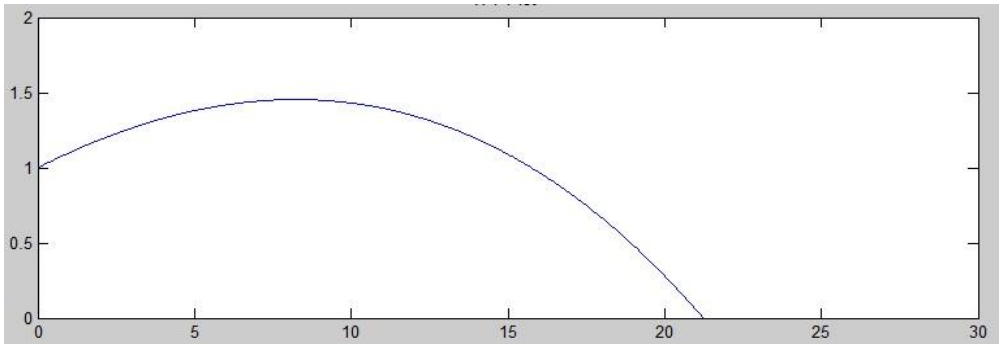

Figure 20. Trajectory in Oxz plane: $\max X = 21.237\ m$, $\max Z = 1.454\ m$.

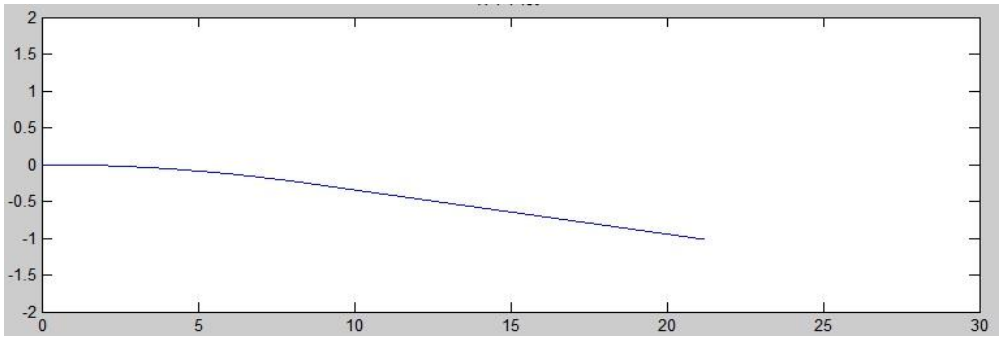

Figure 21. Trajectory in Oxy plane: $\max X = 21.237\ m$, $\min Y = -1.018\ m$.

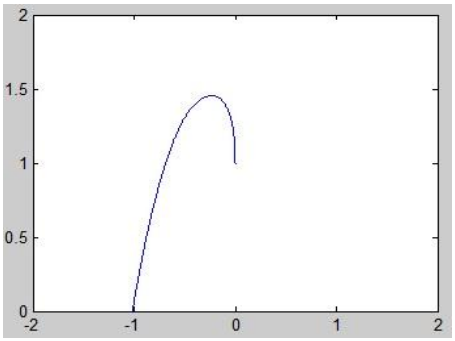

Figure 22. Trajectory in Oyz plane: $\min Y = -1.018\ m$, $\max Z = 1.454\ m$.

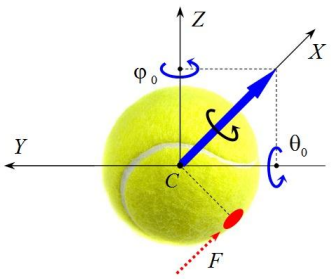

Figure 23. Right backspin stroke: $\theta_0 = -106.066\ s^{-1}$, $\varphi_0 = 106.066\ s^{-1}$.

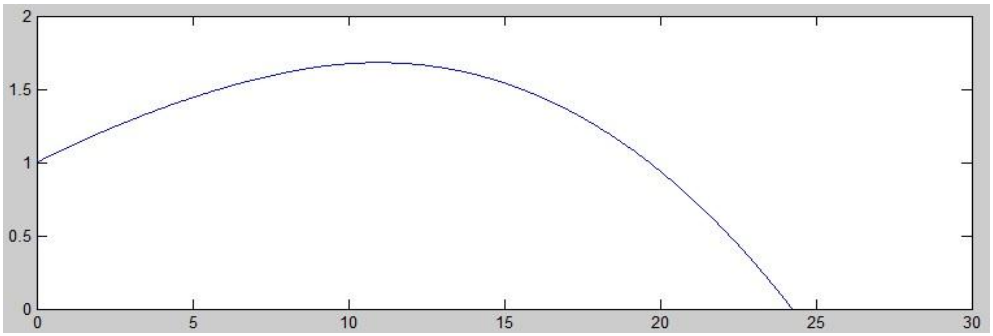

Figure 24. Trajectory in Oxz plane: $\max X = 24.238\ m$, $\max Z = 1.682\ m$.

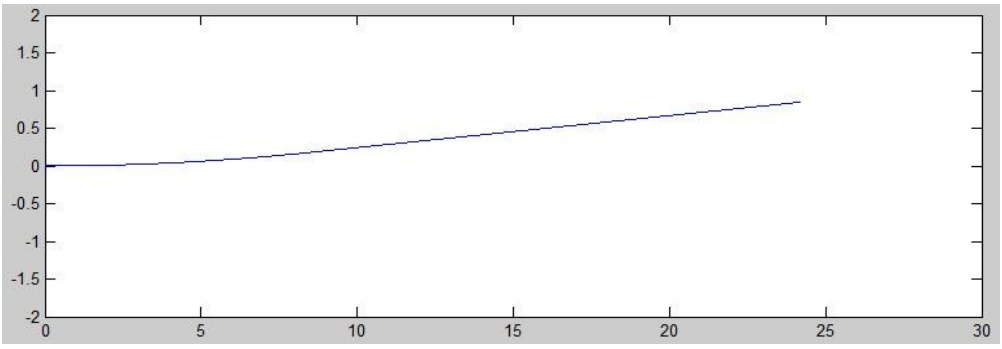

Figure 25. Trajectory in Oxy plane: $\max X = 24.238\ m$, $\max Y = 0.848\ m$.

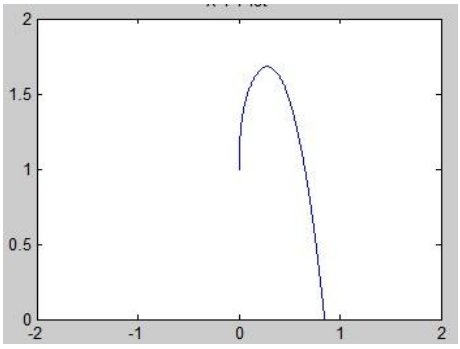

Figure 26. Trajectory in Oyz plane: $\max Y = 0.848\ m$, $\max Z = 1.682\ m$.

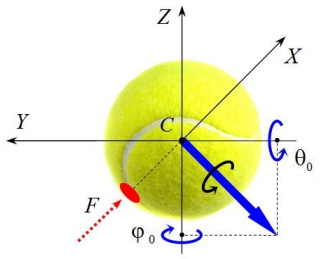

Figure 27. Left backspin stroke: $\theta_0 = -106.066\ s^{-1}$, $\varphi_0 = -106.066\ s^{-1}$.

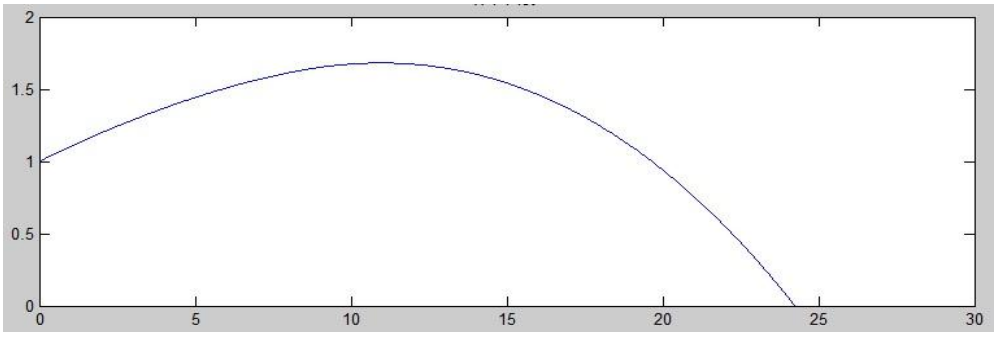

Figure 28. Trajectory in Oxz plane: $\max X = 24.238\ m$, $\max Z = 1.682\ m$.

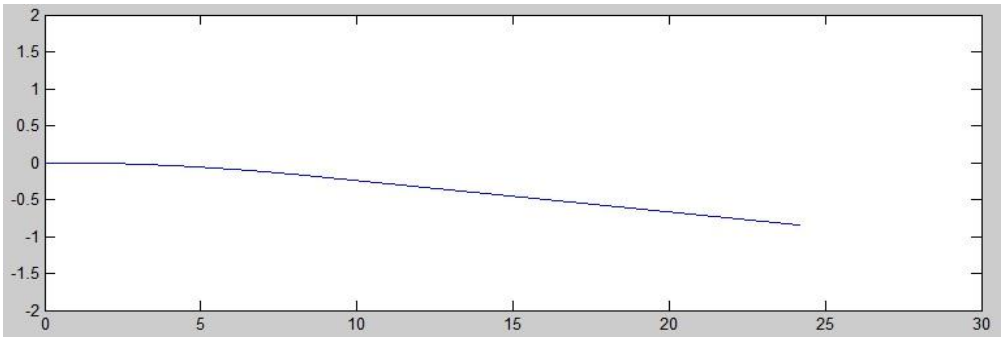

Figure 29. Trajectory in Oxy plane: $\max X = 24.238\ m$, $\min Y = -0.848\ m$.

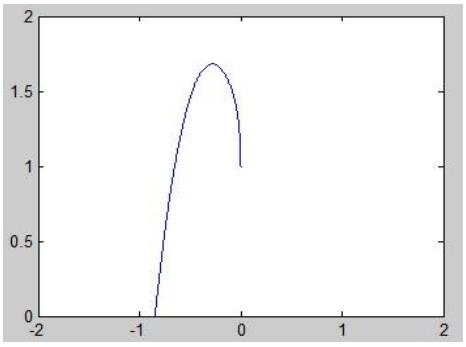

Figure 30. Trajectory in Oyz plane: $\min Y = -0.848\ m$, $\max Z = 1.682\ m$.

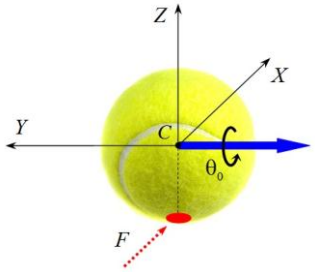

Figure 31. Backspin stroke: $\theta_0 = -150\ s^{-1} \equiv -942.5$ rpm.

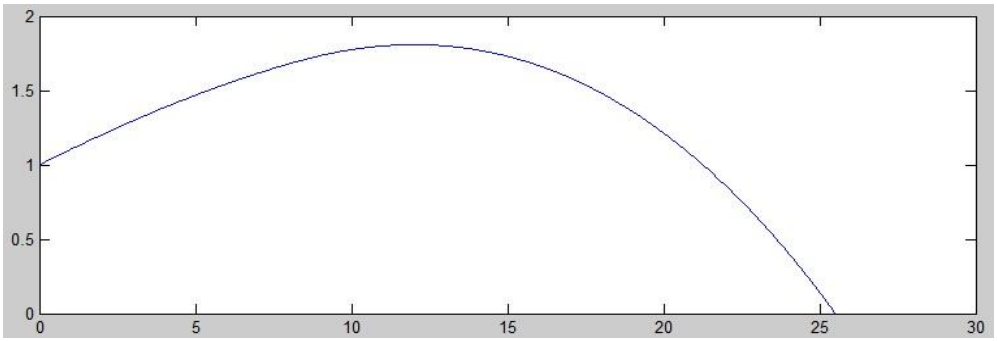

Figure 32. Trajectory in Oxz plane: $\max X = 25.497\ m$, $\max Z = 1.807\ m$.

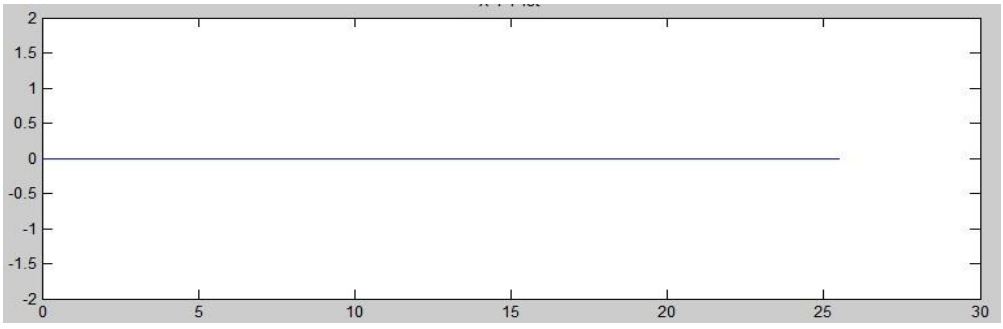

Figure 33. Trajectory in Oxy plane: $\max X = 25.497\ m$, $Y = 0\ m$.

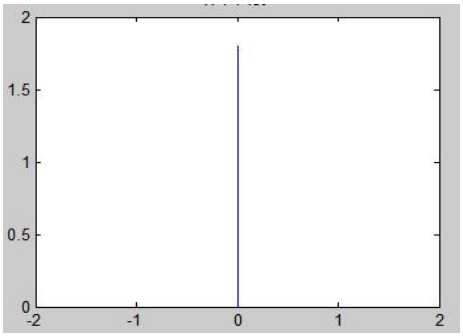

Figure 34. Trajectory in Oyz plane: $Y = 0\ m$, $\max Z = 1.807\ m$.

The eight types of strokes and the corresponding initial angular velocities are:

Topspin stroke: $\dot{\psi}_0 = 0\ s^{-1}$, $\dot{\theta}_0 = 150\ s^{-1}$, $\dot{\varphi}_0 = 0\ s^{-1}$;

Right topspin stroke: $\dot{\psi}_0 = 0\ s^{-1}$, $\dot{\theta}_0 = 106.066\ s^{-1}$, $\dot{\varphi}_0 = 106.066\ s^{-1}$;

Left topspin stroke: $\dot{\psi}_0 = 0\ s^{-1}$, $\dot{\theta}_0 = 106.066\ s^{-1}$, $\dot{\varphi}_0 = -106.066\ s^{-1}$;

Side right-spin stroke: $\dot{\psi}_0 = 0\ s^{-1}$, $\dot{\theta}_0 = 0\ s^{-1}$, $\dot{\varphi}_0 = 150\ s^{-1}$;

Side left-spin stroke: $\dot{\psi}_0 = 0\ s^{-1}$, $\dot{\theta}_0 = 0\ s^{-1}$, $\dot{\varphi}_0 = -150\ s^{-1}$;

Right backspin stroke: $\dot{\psi}_0 = 0\ s^{-1}$, $\dot{\theta}_0 = -106.066\ s^{-1}$, $\dot{\varphi}_0 = 106.066\ s^{-1}$;

Left backspin stroke: $\dot{\psi}_0 = 0\ s^{-1}$, $\dot{\theta}_0 = -106.066\ s^{-1}$, $\dot{\varphi}_0 = -106.066\ s^{-1}$;

Backspin stroke: $\dot{\psi}_0 = 0\ s^{-1}$, $\dot{\theta}_0 = -150\ s^{-1}$, $\dot{\varphi}_0 = 0\ s^{-1}$.

The magnitude of the linear velocity $v_0 = 30\ m/s \equiv 108\ km/h$ and the magnitude of the angular velocity $\omega_0 = 150 s^{-1} \equiv 942.5$ rpm are not chosen randomly.

These parameters correspond to forehand shots and backhand shots, which are performed by professional tennis players. The described strokes, as well as the main parameters of their trajectories, are shown in Figures 3 to 34. As it can be seen from these trajectories, they are arranged according to the length and altitude of the flight under the same initial conditions: the same magnitude of the initial velocity and the same velocity angle towards the horizon. The first stroke, named "Topspin stroke", is a model of an attacking shot in the tennis game, mostly forehand. It has the shortest length because Magnus force is directed mainly downwards and it is summed the force of gravity of the tennis ball. The eighth stroke, named "Backspin stroke", is a model of defensive shot in the tennis game, named a backhand slice. In this stroke, the Magnus force is directed upwards and it is subtracted from the force of gravity of the tennis ball. Thus, this trajectory has the greatest length. In competitive professional tennis, such shots are taken at a very small angle towards the horizon in order to prevent the ball from going out. The other strokes have parameters between these two boundary strokes.

5. Conclusions

The three-dimensional motion of a tennis ball has been studied.

1. The differential equations that describe the three-dimensional motion of a standard tennis ball under given initial conditions are derived.

2. A program for numerical integration of the nonlinear differential equations in the area of the MatLab mathematical package has been compiled.

3. Eight characteristic strokes in tennis at the same initial position, the same magnitude of the initial velocity, and the same initial angle of the velocity vector towards the horizon were studied.

4. The projections of the trajectories of all eight strokes with respect to the three coordinate planes are shown.

5. The research can serve both specialists in the field of Theoretical Mechanics and Aerodynamics, as well as practicing tennis players, including professional athletes and their

coaches.

References

[1] G. Magnus, Über die Abweichung der Geschosse, Abhandlungen der Königlichen Akademie der Wissenschaften zu Berlin, 1852, 1-23.

[2] G. Magnus, Über die Abweichung der Geschosse, und: Über eine abfallende Erscheinung bei rotiernden Körpern, Annalen der Phvsik, 164(1), 1853, 1-29.

[3] Newton, A letter of Mr. Isaac Newton, of the University of Cambridge, Philosophical Transactions of the Royal Societv, Cambridge, 7, 1672, 3075–3087.

[4] B. Robins, New Principles of Gunnery: Containing the Determinations of the Force of Gun-powder and Investigations of the Difference in the Resisting Power of the Air to Swift and Slow Motions, London: J. Nourse, 1742.

[5] R. Cross, Dynamics properties of tennis balls, Physics Department, Sport Engineering, 2, 1999, 23-33.

[6] J. Cooke, An overview of tennis ball aerodynamics, Sport Engineering, 3(2), 2000, 123-129.

[7] R. D. Mehta, J. M. Pallis, Sports ball aerodynamics: effects of velocity spin and surface roughness, Materials and Science in Sports, TMS, 2001, 185-197.

[8] S. G. Chadwick, The aerodynamics properties of tennis balls, The University of Sheffield, Department of Mechanical Engineering, PhD dissertation, 2003, 331.

[9] O. Gonzales, A. B. Graf, J. H. Maddocks, Dynamics of rigid body in a Stockes fluid, Jour. Fl. Mech., 519, 2004, 133-160.

[10] C. Cohen, C. Clanet, Physics of Ball Sports, EPN 47/3, 2016, 13-16.

[11] Li F., Liu L., Wang Q., Qin K., Hu Q., Yang Q., Liu Y., Zhang B., Tennis balls judgment model based on numerical simulation, National Convention on Sports Sc. of Cina, 01018, 2017, 1-3.

[12] F. Alam, A. Subic, J. Naser, M. G. Rasul, M. M. K. Khan, A sydy of sin efects on tennis ball aerodynamics, WSEAS Transactions on Fluid Mechanics, 3(3), 2008, 271-278.

[13] R. Cross, C. Londsey, Masurements of drag and lift on tennis balls in flight, Sports Engineering, 17(2), 2013, 89-96.

[14] S. G. Chadwick, S. J. Haake, The drag coefficient of tennis balls, Engineering of Sport Conference, Sydney, June 2000, 169-176.

[15] S. R. Goodwill, S. B. Chin, S. I. Haake, Aerodynamics of spinning and non-spinning tennis balls, Journ. Wind Eng. and Indust. Aerodyn., 92(11), 2004, 935-958.

[16] R. Mehta, F. Alam, A. Subic, Review of tennis ball aerodynamics. Sports Technology, John Wiley and Sons Asia Pte Ltd, 1, 2008, 1-16.

[17] T. Nakajima, M. Hiratsuka, S. Ito, A. Konno, Aerodynamics characteristics and PIV analyses concerning tennis balls, IOP Conf. Series: Materials Sciene and Eng., 249, 012021, 2017, 1-4.

[18] I. Ivanov, Three-dimensional study of tennis ball flight, Journal Mechanics of Machines, Year XXII, Book 2, 2014, 34-37.